IEEE Access
Multidisciplinary | Rapid Review | Open Access Journal

Received June 9, 2020, accepted June 30, 2020, date of publication July 6, 2020, date of current version July 16, 2020.

Digital Object Identifier 10.1109/ACCESS.2020.3007226

Non-Signalized Intersection Network Management With Connected and Automated Vehicles

XIAOLONG CHEN, BIAO XU, (Member, IEEE), XIAOHUI QIN, YOUGANG BIAN, (Member, IEEE), MANJIANG HU, AND NING SUN

State Key Laboratory of Advanced Design and Manufacturing for Vehicle Body, College of Mechanical and Vehicle Engineering, Hunan University, Changsha 410082, China

Corresponding author: Biao Xu (xubiao@hnu.edu.cn)

This work was supported in part by the Key Research and Development Program of Hunan Province under Grant 2019GK2151 and Grant 2019GK2161, and in part by the State Key Laboratory of Advanced Design and Manufacturing for Vehicle Body under Grant 61775006.

ABSTRACT Road network control is challenging but critical in enhancing urban traffic. This paper proposes a management method for a road network with non-signalized intersections in the connected-vehicle environment, which coordinates connected and automated vehicles' movements to make the non-signalized intersections conflict-free and efficient. Firstly, the proposed method projects vehicles in road networks into virtual platoons and builds the road-network-wide conflict-free geometric topology considering the vehicles' conflicting relationships, which describes the geometry car-following relationship in virtual platoons. Then, a distributed linear controller is designed considering vehicle dynamics and communication topology to organize vehicles' movements with the desired geometric topology. Finally, simulations are conducted to verify the proposed method with different traffic demands. Simulation results show the proposed method can significantly improve traffic efficiency, as well as traffic safety.

INDEX TERMS Connected and automated vehicles, cooperative traffic control, road network, non-signalized intersection, distributed control.

I. INTRODUCTION

Urban traffic is becoming more oppressive with the increase in car ownership, which causes terrible traffic jams and low transportation efficiency. Encouragingly, connected vehicles have been emerging in urban areas in recent years because of the development of advanced wireless communication, which has shown its promising ability to enhance the automation and informatization of traffic management. Researchers are focusing on transportation control methods using connected vehicles to achieve more security, higher throughput and fewer emissions in urban areas. For example, connected-vehicle platoons with a closer car-following distance and smaller traffic-flow fluctuation are adopted to improve traffic throughput in urban roads [1]–[3]. Traffic signal optimization technologies with connected vehicles are utilized to enhance traffic throughput at intersections [4]–[7]. Additionally, with V2X communication, eco-driving systems can obtain sufficient information, such as traffic signals information and vehicles information, which helps decrease fuel consumption and emission further [8]–[10]. Moreover, V2X communication developed for intelligent transportation systems also performs satisfactorily in the safety issue considering it can help avoid collisions at intersections and improve traffic flow stability in road segments [11]–[14].

In urban areas, intersections play an essential role in safety, traffic efficiency, and fuel economy, considering the conflicting merging maneuvers. At an isolated signalized intersection, recent studies have shown that V2I communication can help optimize traffic signals or smooth vehicle speed profiles, thus coordinating the movement of vehicles efficiently. Most research on signalized intersection optimized signal phasing and timing (SPaT) of traffic signals to organize the passing of connected vehicles at intersections, which reduced stops and decelerations [15]–[17]. Another research direction is to plan vehicle speed profiles at signalized intersections with fixed signal timing to avoid unnecessary stops and idlings [18], [19].

Due to the start-up loss and the clearance loss of vehicles in signalized intersections, the traffic signal is not a perfect

The associate editor coordinating the review of this manuscript and approving it for publication was Jianyong Yao.

choice to organize the traffic movement in terms of traffic efficiency. Alternatively, with the automation and information of connected and automated vehicles (CAVs), the conflicting traffic movements at intersections may be separated by space, but not by time, i.e., different signal phases. In other words, the conflicting CAVs can interlace through the intersection without collisions, which can help improve traffic performance further. One notable solution is the so-called non-signalized intersection management, wherein each CAV passes the intersection orderly, forming a self-organized traffic flow. When CAVs enter an intersection, they can exchange information, make decisions, and adjust their positions according to other CAVs. The non-signalized cooperation method for CAVs includes the reservation-based approach, the optimization-based approach, and the virtual platoon based approach. For the reservation-based approach, the vehicle agents submit a spatial-temporal request to the intersection agent to pass the intersection when approaching the intersection, and then the intersection agent agrees or disagrees to this request according to the whole traffic condition in the intersection area [20]–[22]. For the optimization approach, Lee and Park [23] proposed a central optimized control method based on minimum trajectory overlap in which the objective function is the time-displacement trajectory overlap region of conflicting vehicles. However, the central method has a heavy computation burden. To solve this problem, Xu *et al.* [24] proposed a distributed control framework, namely the virtual platoon method. The conflict-free topology was built according to the relationship of traffic order of each vehicle, enabling the vehicles to stagger through the intersection.

Local control for an isolated intersection may not achieve traffic-flow stability in the road network level and may even deteriorate the efficiency of the overall road network. Currently, the studies of traffic optimization in road networks mainly focused on signal optimization, which is just a temporal control of traffic lights. A recent research proposed a cooperative traffic signal control with traffic flow prediction for a 4×4 intersection environment [25]. And Ge *et al.* modeled a multi-intersection traffic network as a multi-agent reinforcement learning system [26]. However, these methods still cannot avoid start-up loss and clearance loss. On the other hand, a few studies focused on the cases of multiple non-signalized intersections. Based on the isolated non-signalized intersection management, Zhang *et al.* [27] developed a model for two adjacent intersections, which provided the possibility of coordinating online a continuous flow of CAVs crossing the intersections. Coincidentally, in [28] a network of three adjacent intersections was explored to estimate the traffic flow where the correlation of the traffic volume between them was analyzed. These studies mostly considered a set of contiguous intersections with two or three intersections. Due to the fact that it was limited to a series of several adjacent intersections, they just simplified the problem with separate vehicles and intersections. It is necessary to further consider a more complicated situation, a grid of intersections, namely a road network. For instance, two case studies with only two intersections and a three by three intersection grid were presented based on mixed integer linear programming for multi-intersection traffic management [29]. Despite of the breakthrough, due to the complex conflict relationship between the vehicles, even all the turns were ignored. Wang *et al.* [30] considered a road network with 6 intersections containing turns lanes where a vehicle needed to receive the trajectories of all other vehicles within the communication range, which needed huge computation resources without considering communication structure. As far as our knowledge, with the increase in the number of controlled intersections, the optimization problem of road network control becomes computationally complex. Moreover, research on how to organize CAVs through the road network is still in its infancy. Existing research does not consider the correlation between isolated intersections. In fact, dynamic vehicle platooning will affect the efficiency of intersection management.

The study is expected to fill the knowledge gap between multiple non-signalized intersections and the impact of connected vehicles. The paper aims to consider the global complex conflict relationship of all approaching vehicles from neighboring intersections in a road network. The focus of this paper is to establish a microscopic traffic model with the conflict-free geometry topology, the communication topology, and the control algorithm as they are implemented at individual vehicles. Therefore, it can achieve safety and efficiency in controlling traffic flow by controlling independent vehicles. We propose a distributed control method framework of CAVs for non-signalized intersection network management. The proposed approach is to construct conflict-free geometric topology for the two-dimensional road network. When considering vehicles from different lanes, the novel method of vehicle group splitting and combination is presented to speed up vehicle convergence to steady state and reduce the computation burden. To achieve distributed control of the topology, the distributed feedback controller is designed. The advantages of the framework include: (1) low complexity of geometric topology for two-dimensional road network; (2) complete consideration of all conflicts from different intersections. Our main contribution of this study is to propose a complete and effective traffic organization method for CAVs in a road network. In order to consider all conflict vehicle relationships and simplify them, we propose vehicle group geometric topology with low complexity wherein vehicle group splitting and combination are designed. The distributed controller is proposed to control vehicles and the stability analysis is verified.

The remainder of the paper is structured as follows. In Section II, we introduce the modeling framework, which includes left and right turns. In Section III, we present the method for vehicle group geometric topology of vehicles at different zones. In Section IV, the distributed controller is designed based on the platoon geometric formation for CAVs in the road network to cross intersections without

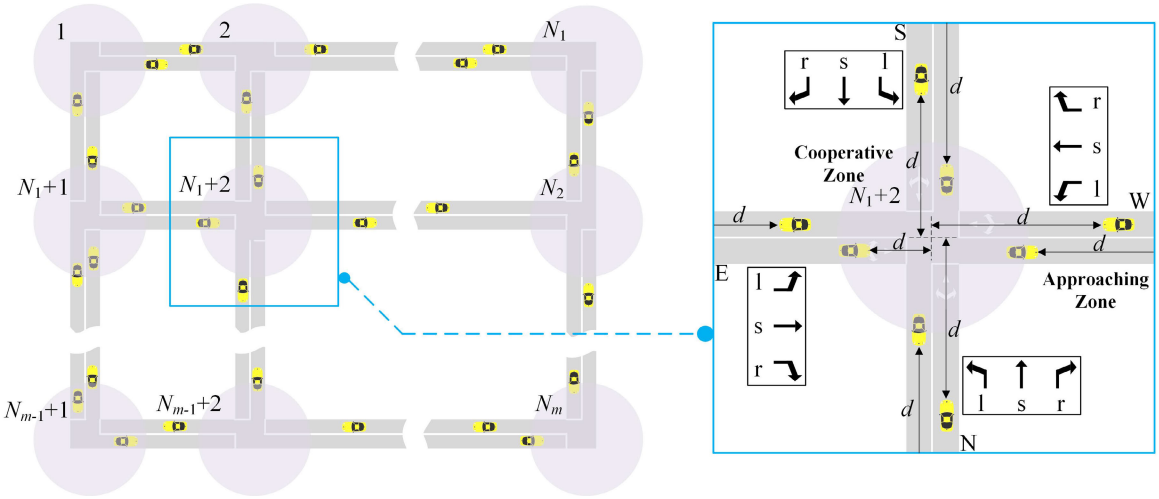

FIGURE 1. Research scene of intelligent and connected vehicle coordination control method in a traffic network.

any movement conflict. In Section V, the system stability is analyzed. Finally, we provide simulation results in Section VI and conclude remarks in Section VII.

II. PROBLEM FORMULATION

The studied scenario is a road network consisting of multiple non-signalized intersections and road segments which is shown in Fig. 1. At each intersection, there is no traffic light. We consider four-leg, one-lane non-signalized intersections, including four entrances and four exits. Each entrance or exit is assumed to contain only one lane. The letters N, W, S, and E represent the four entrance directions heading north, west, south, and east, respectively. The connected vehicles running at the intersections are assumed to be automated vehicles, which could turn left (labeled l), go straight (labeled s), or turn right (labeled r). We assume that the distance between a vehicle and the intersection which the vehicle is heading to is d. When a vehicle passes a certain intersection, the target intersection of the vehicle will change, and the distance to the intersection will be reset to an initial value.

Additionally, each intersection in the road network has two zones, i.e., approaching zone and cooperative zone. The former one allows the vehicle at each entrance to implement a car-following maneuver with its preceding vehicles, called one-dimensional platoon control, whereas the latter one implements two-dimensional vehicle groups coordination control where vehicle adjusts its motion for self-organize and coordinates with others for no-conflict passing intersections.

The range of the cooperative zone of the intersection is determined by the communication distance limit. We consider the vehicle being in the cooperative zone when the vehicle is in the entrance lane of the intersection within the circle. The circle is centered at the center of the intersection and the communication distance is the radius. Otherwise, the vehicle belongs to the approaching zone. On one hand, when the vehicle passes the intersection, its position will switch from the cooperative zone to the approaching zone. On the other hand, when the vehicle enters the communication range at the entrance of the intersection, its position will switch from the approaching zone to the cooperative zone.

Such intersections can well show all the conflict scenes: car-following situation, cross-conflict situation, and confluence situation, which also applies to multi-lane case. Note that this study is not only suitable for this kind of regular road network, but also for other irregular road networks, such as intersections with other shapes and non-straight road networks.

III. VEHICLE GROUP GEOMETRIC TOPOLOGY

Vehicles in the cooperative zone and approaching zone of the intersection are different from car-following states. We use vehicle geometric topology to describe car-following behavior in the road segment and at the intersection, respectively.

A. GEOMETRIC TOPOLOGY FOR VEHICLE PLATOONS IN ROAD SEGMENTS

When the vehicle is in the approaching zone of the road segment, it follows the geometric topology of a one-dimensional vehicle platoon. There are three standard policies of formation geometry for platoon control, as written in [31], namely constant distance policy, constant time headway policy as well as nonlinear distance policy. The objective of these policies is to keep pace with the speed of the preceding vehicle and to maintain the desired distance with neighbor vehicles governed by the inter-vehicle spacing policy:

$$\begin{cases} \lim\limits_{t\to\infty} \left\| v_i(t) - v_{P_i}(t) \right\| = 0 \\ \lim\limits_{t\to\infty} \left(p_{P_i}(t) - p_i(t) - D_i \right) = 0, \end{cases} \tag{1}$$

where v_i and p_i are the velocity and displacement of vehicle i, respectively; P_i is the preceding vehicle of the vehicle i in the same lane; v_{P_i} and p_{P_i} are the velocity and displacement of the vehicle P_i, respectively; D_i is the desired distance. The displacement of vehicle is appointed to the distance between the

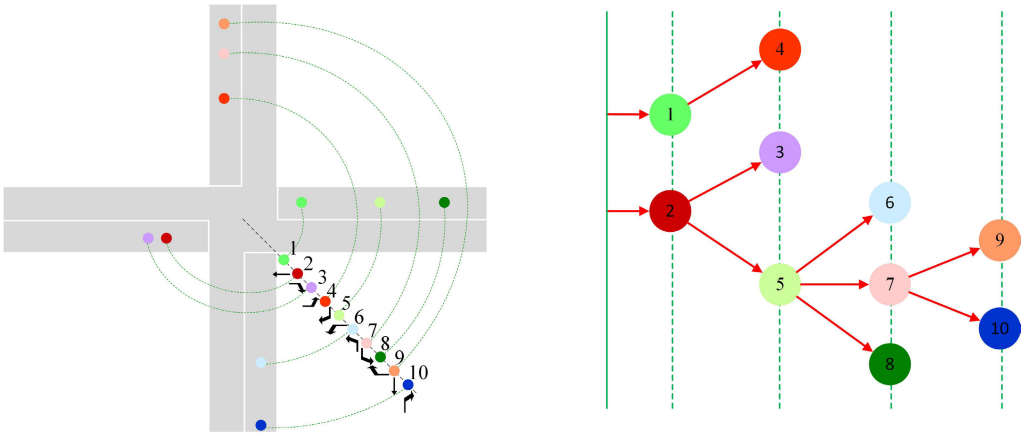

FIGURE 2. Geometric topology.

vehicle and the intersection. Among these following policies, the desired following distance can be as

$$D_i = D_{\mathrm{l}}. \tag{2}$$

$$D_i = t_h v_i + d_0. \tag{3}$$

$$D_i = f\left(v_i\right). \tag{4}$$

where D_{l} is a positive constant value denoting the constant distance in the road segment, t_h is the time headway, d_0 is the minimum following distance and $f(\cdot)$ is the nonlinear function of vehicle velocity denoting nonlinear car-following relation.

Within the approaching zone of the road segment, the vehicle is adjacent to the preceding car in its geometric position. In the formation geometry, to simplify the car-following relationship and achieve high traffic flow density, we decide to use a constant distance policy.

B. GEOMETRIC TOPOLOGY FOR VEHICLE GROUPS AT INTERSECTIONS

The concept of rotation projection was firstly applied in the vehicle group at intersection proposed by Xu *et al.* [24]. Xu *et al.* [24] adopted the rotating projection and the depth-first spanning tree to reconstruct the platoon geometric topology and to obtain a new virtual platoon geometric structure. In this paper, we also use the rotation projection and depth-first spanning tree to construct the geometric topology model of vehicle group at the intersection, as shown in Fig. 2.

In one intersection scenario, sometimes, there is no vehicle in front of vehicle i and having conflict relationship with it. In this case, the conflict vehicle set of it only includes the virtual leading vehicle 0. But there is no virtual leading vehicle in the virtual platoon and conflict-free geometry topology in the road network, which differs from [24]. The leading vehicle is one that has passed the intersection and is running in another road segment. Among the relation of geometry topology for vehicle group at the intersection, there exits car-following relation between vehicle i and its parent node P_i:

$$\begin{cases} \lim\limits_{t\to\infty} \left\| v_i\left(t\right) - v_{P_i}\left(t\right) \right\| = 0 \\ \lim\limits_{t\to\infty} \left(p_{P_i}\left(t\right) - p_i\left(t\right) - D_{\mathrm{i}} \right) = 0, \end{cases} \tag{5}$$

where D_{i} is constant headway at the intersection, which has different value with that for vehicle platoons in road segment.

C. GEOMETRIC TOPOLOGY FOR VEHICLE GROUPS IN ROAD NETWORKS

Based on the geometric topology for road-segment vehicle platoon and vehicle group at the intersection, we can construct the geometric topology for a vehicle group under two-dimensional road network, which is shown in Fig. 3.

On one hand, the leading vehicle of vehicle platoon in the road segment is its preceding vehicle that is within the cooperative zone of the same lane. For example, in Fig. 3, the vehicle platoon in the approaching zone of entrance lane 1 follows the adjacent vehicle (labeled $L_{1,1}$) ahead in the cooperative zone of entrance lane 1. On the other hand, for the virtual vehicle platoon at the intersection, its leading vehicle is the nearest vehicle that has crossed the intersection.

For example, in Fig. 3, the first layer of the virtual platoon at intersection No. 2 includes two vehicle nodes. The first node is going to enter the entrance lane 1 of the intersection No. 1, and the second node is in the direction of one entrance lane of another intersection. In each of the two entrance lanes and the intersection No. 2, there is one nearest neighbor vehicle node (total of 2 vehicle nodes), and the leading vehicle (labeled $L_{v,2}$) of the virtual platoon of the intersection No. 2 is set to be closest to the intersection between the two vehicle nodes.

Through the above geometric topology's construction method of two-dimensional road network vehicle group, the leading vehicle of road-segment vehicle platoon and virtual platoon at the intersection can be determined. Finally, the geometric formation for the vehicle group in the two-dimensional road network is formed. In the geometric topology formation, the following distance D_{l} and D_{i} of the vehicles in the approaching zone and the cooperative zone are different. Due to the convergence of traffic at the intersection, the traffic volume in the cooperative zone is significantly higher than that in the approaching zone. Therefore, in order to ensure the traffic efficiency of the intersection, it is necessary to set the distance D_{i} of the cooperative zone to be small to improve the traffic density of the virtual platoon at

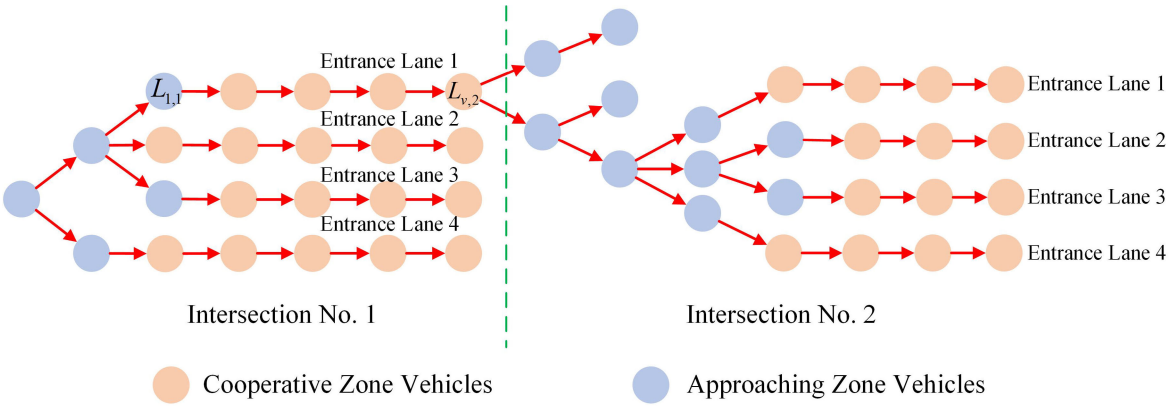

FIGURE 3. Geometric topology for vehicle group in the road network.

the intersection. In this paper, the vehicle set in the approaching zone is defined as $\mathbb{L}$, and the vehicle set in the cooperative zone is defined as $\mathbb{I}$.

In the same vehicle group, the expected distance of the vehicle i from its arbitrary parent node vehicle j can be determined by the vehicle group geometric topology formation. Since the geometric topology of the two-dimensional road network group is a spanning tree, there exists a unique directional path $\{\varepsilon_1, \varepsilon_2, \cdots \varepsilon_n\}$ from node j to node i, where ε_k is an edge in a directed graph. Assuming that there are n_{l} directed edges belonging to the geometric topology of the road segment and n_{I} directed edges belonging to the geometric topology of the intersection. Therefore, the desired following distance between the vehicle i and j is

$$D_{i,j} = n_{\mathrm{l}} D_{\mathrm{l}} + n_{\mathrm{i}} D_{\mathrm{i}}. \tag{6}$$

However, for any node i and j in the same vehicle group, since the geometric topology of the two-dimensional road network group is a spanning tree, it must have a common ancestor node k. Therefore, the desired following distance $D_{i,j}$ between node i and j can be calculated from its desired distance from the ancestor node k:

$$D_{i,j} = D_{i,k} - D_{j,k}. \tag{7}$$

D. VEHICLE GROUP SPLITTING AND COMBINATION

The geometric topology splitting and combination rules mainly consider the car-following distance. When the car-following distance is far in the geometric topology formation of the two-dimensional vehicle group in the road network, in order to prevent the car-following state from converging to steady state for too long, the geometric topology needs to be split. If the vehicle with a longer following distance is located at the intersection cooperative zone, the vehicle and all vehicles behind it in the virtual platoon constitute a new vehicle group, and the new vehicle group topology formation is reconstructed by the mentioned method. On the other hand, if the vehicle with a long following distance is located at the intersection approaching zone, we combine the vehicle and its rear vehicles in the platoon into a new vehicle group, namely reconstructing a new vehicle group topology formation.

Vehicle group splitting is presented in Fig. 4, where the vehicle 6 in the cooperative zone is far away from the vehicle 7 in the cooperative zone; the first vehicle and the second vehicle in the entrance lane 1 in the approaching zone is also far away from each other, so the vehicle group at the intersection is divided into three sub-vehicle groups and three topologies are formed. The three topologies cover the cooperative zone, the approaching zone as well as the region between them, respectively. When the two vehicle groups are close in geometric position, in order to ensure the safety of the two passing through the intersection, the geometric topology needs to be merged. As shown in Fig. 4, if the following distance between vehicle 6 and vehicle 7 decreases into a threshold value, the geometric topology formation of the vehicle group 1 and the vehicle group 2 merge to form a new topological formation.

According to the comparison between the following distance and the threshold value of it, different kinds of vehicle groups are formed when vehicles are split and merged. Jiang *et al.* [32] determined the following threshold according to velocity and headway, finally obtained the optimal following distance threshold 2.5s through data analysis of the vehicle platoon. In this paper, it is assumed that the highest velocity of a vehicle passing the intersection is 20 m/s, and the headway threshold is 2.5s. Therefore, the distance threshold is determined to be about 50m considering the case of CAVs.

In the sub-group after splitting, the head vehicle automatically becomes the leading vehicle of the group, which uniformly speeds up the target traffic speed of v_{T} at the junction and guides the remaining vehicles in the sub-group to pass through the intersection in an orderly manner, thus ensuring traffic efficiency and safety.

IV. DISTRIBUTED CONTROLLER

The information flow topology that characterizes the information transfer between vehicles can be intuitively abstracted into the structure of the graph, and then characterized by the corresponding matrix and its properties. A platoon includes one leading vehicle and N following vehicles as shown in Fig. 4. We introduce a communication topology graph $\bar{\mathcal{G}}_{N+1} = \{\bar{\mathcal{V}}_{N+1}, \bar{\mathcal{E}}_{N+1}\}$ to describe the topological relationship of information where $\bar{\mathcal{V}}_{N+1}$ contains all vehicle nodes and $\bar{\mathcal{E}}_{N+1}$ is the information flow among nodes. In this paper, bidirectional communication is considered,

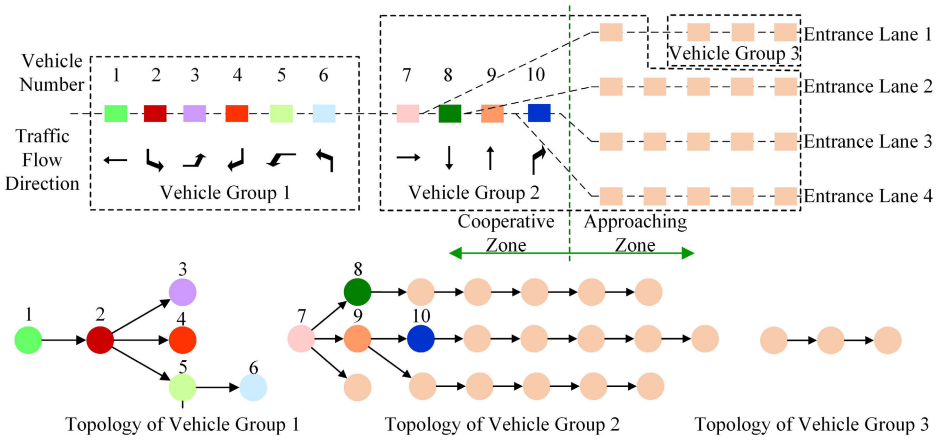

FIGURE 4. Vehicle group splitting.

i.e., if $(i, j) \in \bar{\mathcal{E}}_{N+1}$, we have $(j, i) \in \bar{\mathcal{E}}_{N+1}$. So the communication topology is an undirected graph, and $\bar{\mathcal{E}}_{N+1}$ is an undirected edge.

We introduce the adjacency matrix $\mathcal{A} = [a_{ij}] \in \mathbb{R}^{N\times N}$, and the pining matrix $\mathcal{Q} = [q_{ij}] \in \mathbb{R}^{N\times N}$ to describe the information flow topology.

Adjacency matrix represents information transfer in vehicles except for the leading vehicle:

$$a_{ij} = \begin{cases} 1, & \text{if } (i,j) \in \bar{\mathcal{E}}_{N+1} \\ 0, & \text{else.} \end{cases} \tag{8}$$

Laplacian matrix $\mathcal{L}$ is an extension of adjacency matrix $\mathcal{A}$, which is defined as

$$l_{ij} = \begin{cases} \sum_{k=1}^{N} a_{ik}, & \text{if } i = j \\ -a_{ij}, & \text{else.} \end{cases} \tag{9}$$

The traction matrix $\mathcal{Q}$ is a pair of diagonal arrays, indicating the information transmission of the leading vehicle and the rest of the vehicles, defined as:

$$q_{ij} = \begin{cases} 1, & \text{if } i = j \text{ and } (0,i) \in \bar{\mathcal{E}}_{N+1} \\ 0, & \text{else.} \end{cases} \tag{10}$$

Due to the consideration of bidirectional communication, the adjacency matrix $\mathcal{A}$, Laplacian matrix $\mathcal{L}$, and the traction matrix $\mathcal{Q}$ are all symmetric matrixes.

After feedback linearization, the vehicle nonlinear dynamics model is transformed into a third-order linear dynamic model with first-order inertial links [3]:

$$\dot{p} = -v, \tag{11}$$
$$\dot{v} = a, \tag{12}$$
$$\dot{a} = -\frac{1}{\tau}a + \frac{1}{\tau}u. \tag{13}$$

where $\tau \in \{\tau_e, \tau_b\}$, is the time constant of the first-order inertia link for acceleration response, τ_e is time constant of the first-order inertia link for engine torque response and τ_b is time constant of the first-order inertia link for braking force response.

Denote the status of the vehicle as $\boldsymbol{x} = \begin{bmatrix} p & v & a \end{bmatrix}^T$, the dynamics model of vehicle i can be written as:

$$\dot{\boldsymbol{x}}_i(t) = \boldsymbol{A}\boldsymbol{x}_i(t) + \boldsymbol{B}u_i(t),$$
$$\boldsymbol{x}_i(t) = \begin{bmatrix} p_i \\ v_i \\ a_i \end{bmatrix}, \quad \boldsymbol{A} = \begin{bmatrix} 0 & -1 & 0 \\ 0 & 0 & 1 \\ 0 & 0 & -\frac{1}{\tau} \end{bmatrix}, \quad \boldsymbol{B} = \begin{bmatrix} 0 \\ 0 \\ \frac{1}{\tau} \end{bmatrix}. \tag{14}$$

where $\boldsymbol{x}_i$ is the state of the vehicle i, p_i, v_i and a_i are the distance to the intersection center, speed and acceleration, respectively, u_i is the control variable of the vehicle i - the desired acceleration, τ is the time constant of the acceleration response to the first-order inertia link. Since the homogeneous vehicle virtual platoon is considered, all vehicles have the same coefficient matrices $\boldsymbol{A}$ and $\boldsymbol{B}$.

In this paper, a distributed control architecture of a virtual vehicle platoon is constructed by using the feedback controller based on the following distance error and speed error.

According to the vehicle geometric topology model, the vehicle following distance error and speed error of vehicle i and its neighborhood vehicle j are:

$$\delta_p^{(i,j)} = -\left(p_i(t) - p_j(t) - D\left(l_i - l_j\right)\right), \quad \forall j \in \mathbb{N}_i. \tag{15}$$
$$\delta_v^{(i,j)} = v_i(t) - v_j(t), \quad \forall j \in \mathbb{N}_i. \tag{16}$$

Here, $\mathbb{N}_i$ is the vehicle set in the information neighborhood of vehicle i, which represents the vehicle set can exchange information with vehicle i and is defined in [24], $\delta_p^{(i,j)}$ is the car-following distance error between vehicle i and vehicle j, and $\delta_v^{(i,j)}$ is the car-following speed error between vehicle i and vehicle j, l_i and l_j are the number of layers in the virtual platoon depth-first spanning tree for vehicle i and vehicle j, respectively.

Therefore, the linear feedback control law of the desired acceleration is constructed by a linear combination of the following behavior of the vehicle i and the information from

neighborhood vehicles:

$$\begin{aligned} u_i &= -\sum_{j\in\mathbb{N}_i} k_{p_i}\delta_{\mathrm{p}}^{(i,j)} - \sum_{j\in\mathbb{N}_i} k_{v_i}\delta_{\mathrm{v}}^{(i,j)} \\ &= -k_{p_i}\sum_j a_{ij}\left(p_j(t) - p_i(t) - D\left(l_j - l_i\right)\right) \\ &\quad - k_{p_i}q_{ii}\left(p_0(t) - p_i(t) - D\left(l_0 - l_i\right)\right) \\ &\quad - k_{v_i}\sum_j a_{ij}\left(v_i - v_j\right) - k_{p_i}q_{ii}\left(v_i - v_0\right). \end{aligned} \tag{17}$$

where k_{p_i} and k_{v_i} are the feedback gains of the distance error and velocity error of the linear feedback controller of the vehicle i, respectively, and u_i is the controller input of the vehicle, that is, the desired acceleration.

By introducing the car following model, taking the following error of the vehicle i and the virtual leading vehicle as a new state variable, i.e.,

$$\bar{\boldsymbol{x}}_i = \begin{bmatrix} \bar{x}_{i,1} \\ \bar{x}_{i,2} \\ \bar{x}_{i,3} \end{bmatrix} = \begin{bmatrix} p_0 - p_i - D\left(l_0 - l_i\right) \\ v_i - v_0 \\ a_i \end{bmatrix}, \quad \forall i \in \{1, 2, \cdots, N\}. \tag{18}$$

The control variable $\bar{u}_i$ is the expected acceleration u_i of the vehicle i, i.e., $\bar{u}_i = u_i$.

Then the car following dynamics equation is

$$\dot{\bar{x}}_i = \boldsymbol{A}\bar{x}_i + \boldsymbol{B}\bar{u}_i, \quad \forall i \in \{1, 2, \cdots, N\}. \tag{19}$$

Thus, the linear feedback law is converted to

$$\begin{aligned} \bar{u}_i &= -k_{p_i}\sum_j a_{ij}\left(\bar{x}_{i,1} - \bar{x}_{j,1}\right) \\ &\quad - k_{p_i}q_{ii}\bar{x}_{i,1} - k_{v_i}\sum_j a_{ij}\left(\bar{x}_{i,2} - \bar{x}_{j,2}\right) - k_{p_i}q_{ii}\bar{x}_{i,2} \\ &= -k_{p_i}\sum_j \left(l_{ij} + q_{ij}\right)\bar{x}_{j,1} - k_{v_i}\sum_j \left(l_{ij} + q_{ij}\right)\bar{x}_{j,2}. \end{aligned} \tag{20}$$

Let $\boldsymbol{k}_i = \boldsymbol{k} = \left[k_p, k_v, 0\right]^T$, so there is

$$\bar{u}_i = -\sum_j \left(l_{ij} + q_{ij}\right)\boldsymbol{k}^T\bar{x}_j, \quad \forall i \in \{1, 2, \cdots, N\}. \tag{21}$$

V. INTERNAL STABILITY ANALYSIS

This section focuses on the stability analysis of a homogeneous vehicle platoon based on the aggregated dynamics model.

A. AGGREGATED DYNAMIC MODEL

In order to derive the overall closed-loop dynamics model of the platoon, an aggregated systems state $\boldsymbol{X} = \left[\bar{\boldsymbol{x}}_1^T, \bar{\boldsymbol{x}}_2^T, \cdots, \bar{\boldsymbol{x}}_N^T\right]^T$ and an aggregated input $\boldsymbol{U} = \left[\bar{u}_1, \bar{u}_2, \cdots, \bar{u}_N\right]^T$ are defined. The system dynamics can be expressed as,

$$\begin{aligned} \dot{\boldsymbol{X}} &= \bar{\boldsymbol{A}}\boldsymbol{X} + \bar{\boldsymbol{B}}\boldsymbol{U}, \\ \boldsymbol{U} &= -\bar{\boldsymbol{C}}\boldsymbol{X}. \end{aligned} \tag{22}$$

where (23)–(25), as shown at the bottom of the page, where $\otimes$ denotes Kronecker product.

Hence, the system dynamics equation with a given information flow topology can be written in the following compact form

$$\begin{aligned} \dot{\boldsymbol{X}} &= \boldsymbol{I}_N \otimes \boldsymbol{A} \cdot \boldsymbol{X} - \boldsymbol{I}_N \otimes \boldsymbol{B} \cdot \left(\mathcal{L} + \mathcal{Q}\right) \otimes \boldsymbol{k}^T \cdot \boldsymbol{X} \\ &= \left(\boldsymbol{I}_N \otimes \boldsymbol{A} - \left(\boldsymbol{I}_N \otimes \boldsymbol{B}\right) \cdot \left(\left(\mathcal{L} + \mathcal{Q}\right) \otimes \boldsymbol{k}^T\right)\right)\boldsymbol{X}. \end{aligned} \tag{26}$$

According to the hybrid product properties of the Kronecker product, we have

$$\begin{aligned} \left(\boldsymbol{I}_N \otimes \boldsymbol{B}\right) \cdot \left(\left(\mathcal{L} + \mathcal{Q}\right) \otimes \boldsymbol{k}^T\right) &= \left(\boldsymbol{I}_N\left(\mathcal{L} + \mathcal{Q}\right)\right) \otimes \left(\boldsymbol{B}\boldsymbol{k}^T\right) \\ &= \left(\mathcal{L} + \mathcal{Q}\right) \otimes \left(\boldsymbol{B}\boldsymbol{k}^T\right). \end{aligned}$$

(26) can be rewritten as

$$\dot{\boldsymbol{X}} = \left(\boldsymbol{I}_N \otimes \boldsymbol{A} - \left(\mathcal{L} + \mathcal{Q}\right) \otimes \left(\boldsymbol{B}\boldsymbol{k}^T\right)\right)\boldsymbol{X}. \tag{27}$$

Here, $\boldsymbol{A}$ and $\boldsymbol{B}$ are the vehicle longitudinal dynamics, $\mathcal{L}$ and $\mathcal{Q}$ express the information flow topologies, $\boldsymbol{X}$ indicates the no-conflict geometry topology of the virtual platoon, and $\boldsymbol{k}^T$ displays the decentralized feedback control law.

B. SYSTEM STABILITY ANALYSIS

The closed-loop stability of the system will be analyzed based on (27) through graph theory, Routh-Hurwitz stability criterion, and matrix eigenvalue analysis. The system (27) can be said to be internal stable by properly choosing the feedback gains $\boldsymbol{k}^T$ if and only if all real part of the eigenvalues of $\boldsymbol{I}_N \otimes \boldsymbol{A} - \left(\mathcal{L} + \mathcal{Q}\right) \otimes \left(\boldsymbol{B}\boldsymbol{k}^T\right)$ are negative [33].

Lemma 1: Consider a matrix $\mathcal{M} = \left(m_{ij}\right) \in \mathbb{R}^{N\times N}$ and a set $J = \left\{i \in \{1, 2, \ldots, N\} \,|\, |m_{ii}| > \sum_{i=1, j\neq i}^{n} \left|m_{ij}\right|\right\} \neq \emptyset$. If for each $i \notin J$, there exists a nonzero sequence $\left\{m_{ii_1}, m_{i_1i_2}, \ldots, m_{i_rj}\right\}$ of $\mathcal{M}$ with $j \in J$, then $\mathcal{M}$ is nonsingular [34].

$$\bar{\boldsymbol{A}} = \boldsymbol{I}_N \otimes \boldsymbol{A} \in \mathbb{R}^{3N\times 3N}, \tag{23}$$

$$\bar{\boldsymbol{B}} = \boldsymbol{I}_N \otimes \boldsymbol{B} \in \mathbb{R}^{3N\times N}, \tag{24}$$

$$\begin{aligned} \bar{\boldsymbol{C}} &= \begin{bmatrix} \left(l_{11} + q_{11}\right)\boldsymbol{k}^T & \left(l_{12} + q_{12}\right)\boldsymbol{k}^T & \cdots & \left(l_{1N} + q_{1N}\right)\boldsymbol{k}^T \\ \left(l_{21} + q_{21}\right)\boldsymbol{k}^T & \left(l_{22} + q_{22}\right)\boldsymbol{k}^T & \cdots & \left(l_{2N} + q_{2N}\right)\boldsymbol{k}^T \\ \vdots & \vdots & \ddots & \vdots \\ \left(l_{N1} + q_{N1}\right)\boldsymbol{k}^T & \left(l_{N2} + q_{N2}\right)\boldsymbol{k}^T & \cdots & \left(l_{NN} + q_{NN}\right)\boldsymbol{k}^T \end{bmatrix} \\ &= -\left(\mathcal{L} + \mathcal{Q}\right) \otimes \boldsymbol{k}^T \in \mathbb{R}^{N\times 3N}, \end{aligned} \tag{25}$$

Theorem 1: The communication matrix $\mathcal{L}+\mathcal{Q}$ is a real and positive matrix.

Proof: From the definitions of $\mathcal{L}$ and $\mathcal{Q}$ in (8), (9) and (10), we can know that both the $\mathcal{L}$ and $\mathcal{Q}$ are real symmetric matrices, so $\mathcal{L}+\mathcal{Q}$ is also a real symmetric matrix. Therefore, the characteristic roots of $\mathcal{L}+\mathcal{Q}$ are real numbers.

According to **Gersgorin Disk Criterion** [35], all the eigenvalues of the $\mathcal{L}+\mathcal{Q}$ matrix are located in the union of N disks

$$\bigcup_{i=1}^{N}\{\lambda\in\mathbb{C}\lambda-l_{ii}-q_{ii}|\leq\sum_{j=1,j\neq i}^{N}|l_{ij}|\}. \tag{28}$$

In addition, since $\sum_{j=1,j\neq i}^{N}|l_{ij}|=\sum_{j=1,j\neq i}^{N}|a_{ij}|=l_{ii}\leq l_{ii}+q_{ii}\,(>0)$, we can have $|\lambda-(l_{ii}+q_{ii})|\leq l_{ii}+q_{ii}$. Therefore, for $\mathcal{L}+\mathcal{Q}$, all the eigenvalues lie within the union

$$\{\lambda\in\mathbb{C}|\mathrm{Re}(\lambda)>0\cup\{0\}\}. \tag{29}$$

Besides, according to the condition of the directed spanning tree, there is at least one following node that can obtain the information of the leading node. Think of $\mathcal{L}+\mathcal{Q}$ as $\mathcal{M}$ defined in Lemma 1, then $J=\left\{i\in\{1,2,\ldots,N\}\,|\,|l_{ii}+q_{ii}|>\sum_{i=1,j\neq i}^{N}|l_{ij}+q_{ij}|\right\}$. Since $|l_{ii}+q_{ii}|=\sum_{i=1,j\neq i}^{N}a_{ij}+q_{ii}$ and $\sum_{i=1,j\neq i}^{N}|l_{ij}+q_{ij}|=\sum_{i=1,j\neq i}^{N}|l_{ij}|=\sum_{i=1,j\neq i}^{N}a_{ij}$, we can have $J=\{i\in\{1,2,\ldots,N\}|q_{ii}>0\}$. Therefore, $i\notin J\Leftrightarrow i\in\{i|q_{ii}=0\}$, which means i cannot communicate with the leader. But there must be at least one directed path from node $j\in J$ to node i, and there exists a nonzero sequence $\left\{l_{ii_1}+q_{ii_1},l_{i_1i_2}+q_{i_1i_2},\ldots,l_{i_rj}+q_{i_rj}\right\}$ in $\mathcal{L}+\mathcal{Q}$. Thus, according to Lemma 1, $\mathcal{L}+\mathcal{Q}$ is nonsingular, which implies all the eigenvalues of $\mathcal{L}+\mathcal{Q}$ are real and positive. ■

Theorem 2: the stability of (27) is equivalent to that $\boldsymbol{A}-\lambda_i\boldsymbol{B}\boldsymbol{k}^T,\forall i\in N$ are Hurwitz matrices.

Proof: There is a non-singular matrix $\boldsymbol{P}$, we have

$$\boldsymbol{P}^{-1}(\mathcal{L}+\mathcal{Q})\boldsymbol{P}=\boldsymbol{J}.$$

where $\boldsymbol{J}$ is Jordan normal form of $\mathcal{L}+\mathcal{Q}$.

Since both $\boldsymbol{P}$ and $\boldsymbol{I}_N$ can be reversed, it can be known that $\boldsymbol{P}\otimes\boldsymbol{I}_N$ is reversible according to the Kronecker product property. A similar transformation is performed on $\boldsymbol{A}_c=\boldsymbol{I}_N\otimes\boldsymbol{A}-(\mathcal{L}+\mathcal{Q})\otimes\boldsymbol{B}\boldsymbol{k}^T$:

$$(\boldsymbol{P}\otimes\boldsymbol{I}_N)^{-1}\boldsymbol{A}_c(\boldsymbol{P}\otimes\boldsymbol{I}_N)=\boldsymbol{I}_N\otimes\boldsymbol{A}-\boldsymbol{J}\otimes\left(\boldsymbol{B}\boldsymbol{k}^T\right).$$

Thus, $\boldsymbol{I}_N\otimes\boldsymbol{A}-\boldsymbol{J}\otimes\left(\boldsymbol{B}\boldsymbol{k}^T\right)$ is a block upper triangular matrix. $\boldsymbol{A}_c$ and $\boldsymbol{I}_N\otimes\boldsymbol{A}-\boldsymbol{J}\otimes\left(\boldsymbol{B}\boldsymbol{k}^T\right)$ are similar matrices and have the same eigenvalues. ■

Therefore, the eigenvalues of $\boldsymbol{A}_c$ are the roots of (30).

$$\left|\lambda\boldsymbol{I}_{3N}-\left(\boldsymbol{A}-\boldsymbol{J}\otimes\left(\boldsymbol{B}\boldsymbol{k}^T\right)\right)\right|=\prod_{i=1}^{r}\left|\lambda\boldsymbol{I}_3-\boldsymbol{A}+\lambda_i\boldsymbol{B}\boldsymbol{k}^T\right|^{n_i}=0. \tag{30}$$

And the characteristic polynomial of the matrix is

$$\left|\lambda\boldsymbol{I}_3-\boldsymbol{A}+\lambda_i\boldsymbol{B}\boldsymbol{k}^T\right|=\lambda^3+\frac{\lambda^2}{\tau}+\frac{k_v\lambda_i\lambda}{\tau}+\frac{k_p\lambda_i}{\tau}.$$

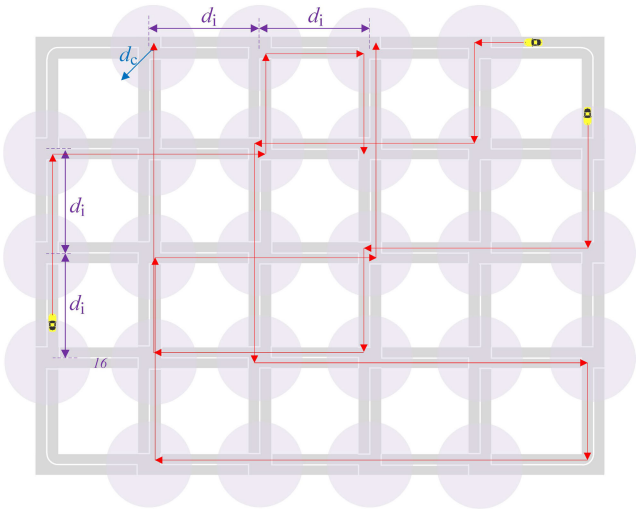

FIGURE 5. Test scenario.

We use the Routh-Hurwitz criterion to test its stability and the characteristic roots λ_i of $\mathcal{L}+\mathcal{Q}$ are all positive real numbers, therefore

$$k_v>0,\quad k_p>0,\ k_v>\tau k_p. \tag{31}$$

VI. SIMULATION AND ANALYSIS

In this section, numerical simulations of the proposed distributed cooperative control method for CAVs at the non-signalized intersection network are conducted in the Simulation of Urban Mobility (SUMO) [36] to test the performance with different traffic demands.

A. BENCHMARK ALGORITHM

We adopt the reservation-based intersection cooperative control method with a First-Come-First-Serve (FCFS) policy [21], [37] as the benchmark algorithm. The algorithm can present the FCFS principle and spatiotemporal resource allocation well and is easily expanded to a road network.

In the reservation-based method, vehicles use the FCFS policy to schedule the time to pass the intersection under the management of the traffic controller. The approaching vehicles apply the time-duration reservation from the traffic controller to pass the intersection. If the applied time duration has been occupied, the traffic controller rejects the vehicle reservation request, and the vehicle decelerates and re-reserve the time duration to pass the intersection. In the reservation-based method, the vehicle reservation distance and the vehicle safety distance are important parameters therein. In the simulation, the vehicle reservation distance and the vehicle safety distance are set to be consistent with the coordination distance and the desired following distance of the proposed method in this paper, respectively.

B. TESTING SCENARIOS

We use a typical small traffic network of 5×6 as the simulation scenario, as shown in Fig. 5. In the test scenario, there are 26 intersections (the intersections at the corners

TABLE 1. Simulation scenarios.

Average Head Distance (m/veh)	30	40	50	60	70	80	90	100	110	120	130	140	150
Traffic Density (veh/km)	33	25	20	17	14	12.5	11	10	9	8	7.7	7	6.7

can be considered as road segments) and 90 road segments, including 12 crossroads and 14 T-junctions. Set the distance between adjacent intersections in the traffic network to be d_{i}, that is, the length of the link connecting the intersections is d_{i}. For each intersection, the communication distance is d_{c}, which is equal to the coordination distance. When vehicles enter the intersection communication distance, the virtual platoon is constructed by the intersection geometry. Otherwise, when vehicles are outside the intersection communication distance, the actual vehicle topology is constructed. In the simulation, d_{i} is set to be 1km and d_{c} is set to be 500m.

In the constructed traffic network, several vehicles are randomly generated on each road segment with a certain average density k_f, and the initial velocities of vehicles are randomly distributed according to the normal distribution of $\mathcal{N}\left(15, 1.5^2\right)$. The initial headway distances of vehicles are randomly generated according to the normal distribution $\mathcal{N}\left(\mu, \sigma^2\right)$, where the expectation and variance of the head distances are related to the density of the traffic flow in the road network, respectively:

$$\mu = \frac{1}{k_f}, \quad \sigma = 0.15\mu.$$

Vehicles always travel within the road network during the simulation time, ensuring that the average density of the vehicles in the traffic network remains constant during the simulation time. When vehicles travel to the intersections, the probability of traveling to each exit lane of the intersection is equal, and the travel trajectory is determined in the simulation initialization procedure. The red lines show the typical travel trajectory of three randomly generated vehicles in Fig. 5.

In the simulation, 13 simulation scenarios with different traffic flow densities are set in TABLE 1. The expectations of the head distances are: 30 m/veh, 40 m/veh, 50 m/veh, 60 m/veh, 70 m/veh, 80 m/veh, 90 m/veh, 100 m/veh, 110 m/veh, 120 m/veh, 130 m/veh, 140 m/veh, and 150 m/veh, respectively. The corresponding traffic densities are shown in TABLE 1 which represents the low, medium and high traffic volume conditions, respectively. In the traffic simulation scenario, the proposed method and the benchmark algorithm are used as the comparison algorithms to simulate, record, and output the vehicle motion information, and we use the same vehicle model to calculate the fuel consumption and average speed, etc., as performance indicators. In all simulations, the inertial lag of vehicle τ is 0.5 s. And the feedback gains of the distance error k_p and velocity error k_v of the linear feedback controller are 0.15 and 0.7, respectively. We count the total computation time of the geometry topology construction of the virtual platoon and the control input calculation of a single vehicle, of which the results show

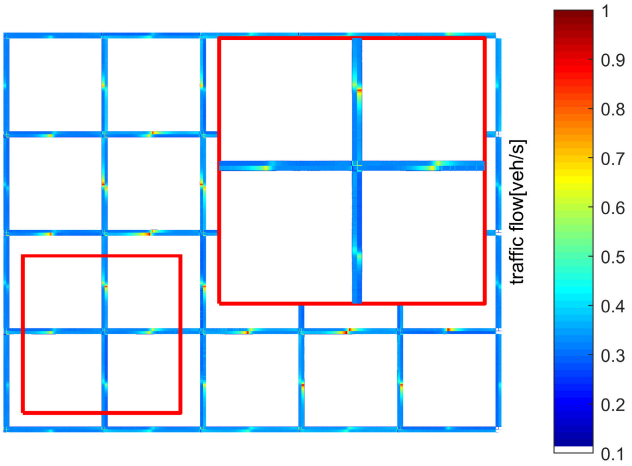

FIGURE 6. Road network traffic flow density with cooperative control method under medium flow condition.

that the average and maximum time costs on computation are almost 0.004 s and 0.008 s, respectively, which proves the low computation complexity of the proposed method.

C. CASE STUDY

We first show the results of one case study with the medium flow condition (12.5 veh/km, the expectation of the head distance is 80 m/veh) as an example to show the average traffic flow density thermogram and the average vehicle velocity profile. Wherein, the average traffic flow density value of a point in the road network is the total number of vehicles occupying over a unit distance of the point divided by the total simulation time. The average speed of a point in the road network is the average of the speeds of all vehicles at that point over a unit distance.

Fig. 6 and Fig. 8 are the heat flow diagrams of traffic flow density distribution in the road network for the proposed method and the benchmark algorithm under medium flow condition. It can be seen from the figures that the density of vehicles in the proposed method is evenly distributed in the road network. Even the density near the boundary between the coordinated area and the non-coordinating area is small, and no serious congestion occurs. In the benchmark algorithm, the vehicle density is unevenly distributed in the road network, and the road segment area in the road network is sparse. However, in the road network, the intersection area is dense. As the density increases sharply near the intersection, the traffic congestion problem is more serious. Fig. 7 and Fig. 9 are the spatial distribution of traffic flow velocity in the road network for the proposed method and the benchmark algorithm under the medium flow condition. It can be seen from the figures that the speed of the vehicles is more consistent in the traffic network in the proposed

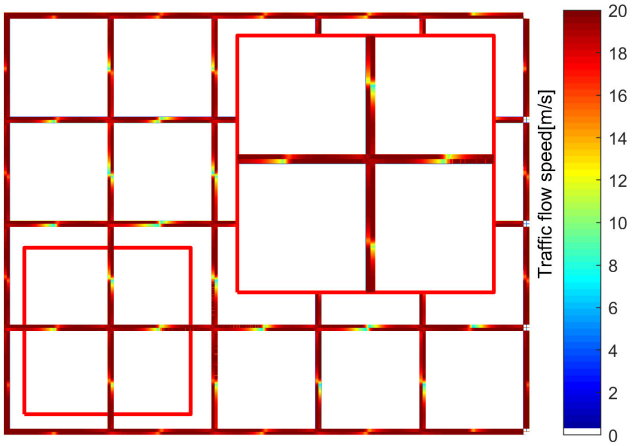

FIGURE 7. Road network traffic flow velocity with cooperative control method under medium flow condition.

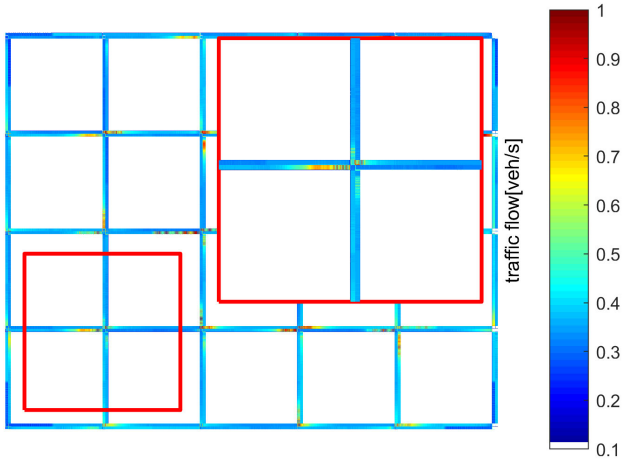

FIGURE 8. Road network traffic flow density with benchmark algorithm under medium flow condition.

method due to considering the information of neighboring vehicles. The speed is reduced near the boundary between the coordinated area and the non-coordinating area, but the size of the area where the speed is reduced is smaller and the reduction is smaller. So we can see that the vehicle ensures the high speed of entering the cooperative zone by finely adjusting the speed when crossing the approaching zone to the cooperative zone, which proves our method has the ability to coordinate the vehicle to converge faster in the transition area. In the benchmark algorithm, the vehicle speed is poorly distributed in the road network, because vehicles have to constantly adjust their speed to get reservations. The flow rate in the road segment of the road network is large, the flow velocity in the intersection area is significantly reduced, and the flow reduction area is significantly expanded compared with the coordinated control method, and the traffic congestion problem is more serious.

Trajectories of vehicles in lane 16 (see Fig. 5) for 80 m/veh traffic demand in the cooperative control method and the benchmark algorithm are shown in Fig. 10 and Fig. 11, respectively, where the x-axis shows the

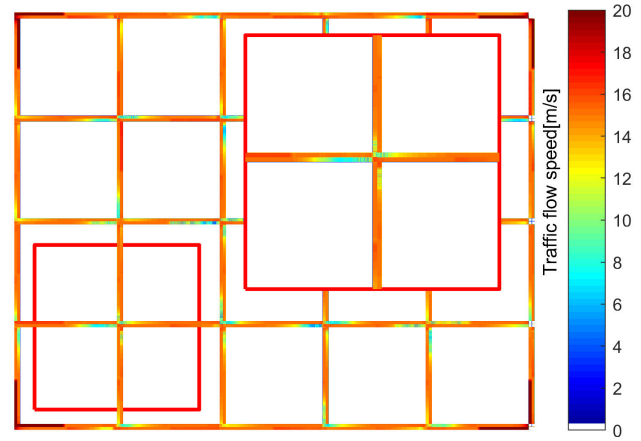

FIGURE 9. Road network traffic flow velocity with benchmark algorithm under medium flow condition.

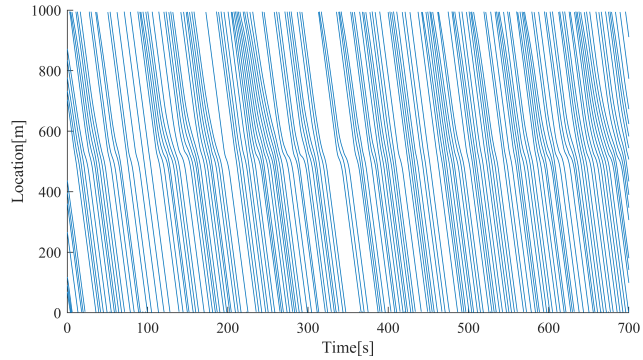

FIGURE 10. Trajectories of vehicles in lane 16 for 80 m/veh traffic demand in the cooperative control method.

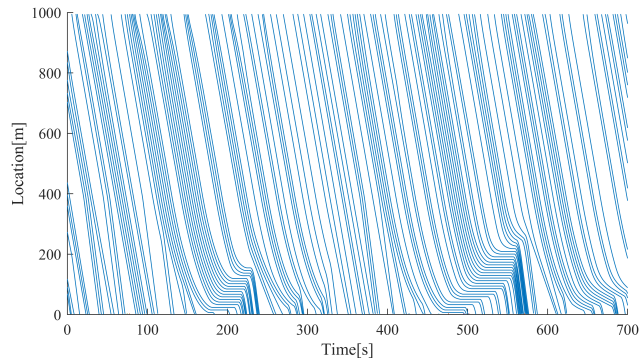

FIGURE 11. Trajectories of vehicles in lane 16 for 80 m/veh traffic demand in the benchmark algorithm.

intersection location. Vehicles travel at their desired speed and maintain a safe distance with potentially colliding vehicles according to different methods. It can be found in Fig. 10 that the cooperative control method requires almost no waiting. The speed adjustment occurs at the junction of the cooperative zone and approaching area, but still passes at a higher speed, and the distribution of the entire vehicle is relatively uniform. Moreover, it is because of the slight adjustment of the speed of the vehicle that the vitality of the entire system is maintained. But the trajectories of vehicles shown in Fig. 11 have large fluctuations. It is apparent

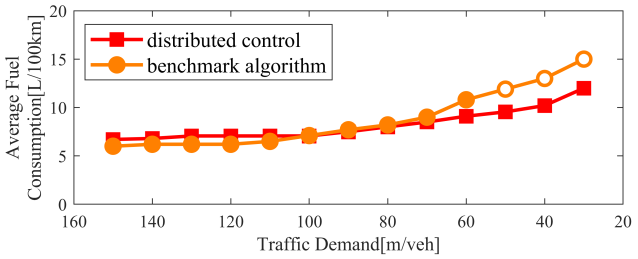

FIGURE 12. Average fuel consumption under different traffic density.

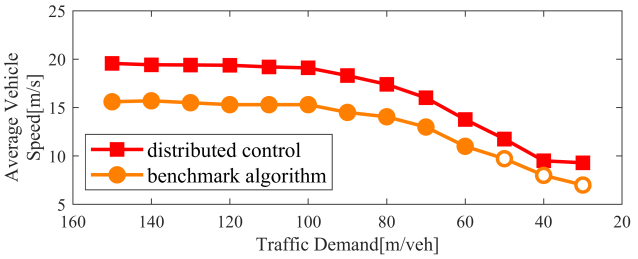

FIGURE 13. Average vehicle speed under different traffic density.

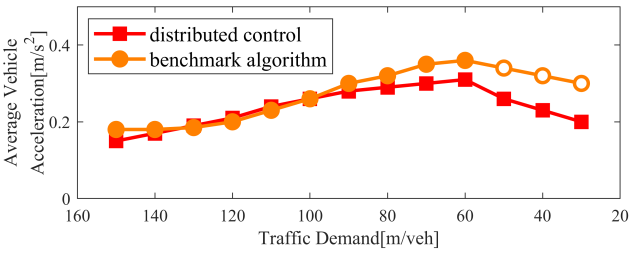

FIGURE 14. Average vehicle acceleration under different traffic density.

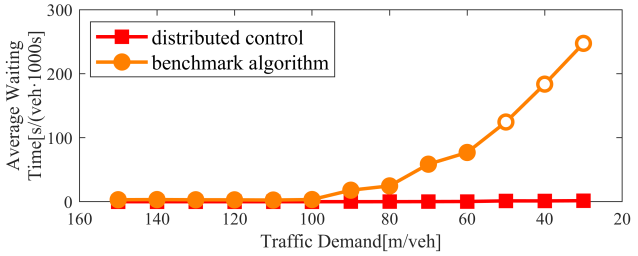

FIGURE 15. Average waiting time under different traffic density.

that some vehicles stop in the approaching zone near the intersection. And in higher traffic flows, the situation is more serious.

Therefore, under the medium traffic flow condition, the cooperative control method can effectively reduce the fluctuation of traffic flow speed and the uniformity of traffic density, and significantly improve the traffic efficiency of the road network.

D. STATISTICAL RESULTS OF DIFFERENT TRAFFIC DENSITIES

Fig. 12 - Fig. 15 show the curves of the average fuel consumption, average speed, average acceleration, and average waiting time for per vehicle in 1000 seconds under different traffic demands. Since the number of vehicles involved in a collision is over 100 when the traffic density is greater than 50 m/veh, we mark them with hollow circles. From the results, we can see that the distributed control method can keep traffic running without collisions in all kinds of traffic demand, which proves that the proposed can improve traffic safety.

As can be seen from Fig. 12, the distributed control method can improve the fuel economy of vehicles at high traffic densities compared to the benchmark algorithm. The vehicle fuel consumption of the distributed control method increases slowly linearly with the increase in traffic density when the traffic density is less than 110 m/veh. The vehicle fuel consumption of the benchmark algorithm has the same trend and these values are almost the same. When the traffic density is greater than 100 m/veh, the traffic congestion increases, and the fuel consumption of the benchmark algorithm increases with the increase in traffic flow and exceeds the value of the distributed control method. Although the overall difference is not a bit at first, the benchmark algorithm deteriorates faster than the proposed algorithm when the traffic density is greater than 70 m/veh.

As can be seen from Fig. 13, the distributed control method can improve the average vehicle speed, that is, traffic efficiency, at different traffic densities than the benchmark algorithm. Similar to the fuel consumption of the vehicle, the average vehicle speed of the distributed control method decreases slowly linearly with the increase of traffic flow when the traffic density is less than 100 m/veh, and when the traffic density is greater than 100 m/veh, the traffic congestion is aggravated. The distributed control method shows the possibility of maintaining a speed of around 10 m/s at high traffic density. The average speed shows an approximate exponential decline with increasing traffic flow. The average speed of the vehicle in the benchmark algorithm shows an approximate exponential decline after the traffic density is greater than 100 m/veh. When the traffic density is higher, the average speed continues to drop.

As can be seen from Fig. 14, the average acceleration of vehicles in distributed control increases with the increase of density when the traffic density is less than 60 m/veh. The average speed of the vehicle decreases when the traffic density is greater than 60 m/veh, and the congestion increases, therefore, the average acceleration is instead reduced. The turning point of the benchmark algorithm is roughly 70 m/veh. The more the number of vehicles, the more crowded, the less likely the vehicle is to get the reservation by adjusting the speed. Thus, the average acceleration is getting higher than that in the distributed control.

In Fig. 15, the average waiting time is the accumulated time within the previous time interval of length 1000s divided by the number of vehicles in the traffic network. As can be seen from the figure, the average waiting time in distributed control is almost zero. The cooperative distributed control method adjusts vehicles speed and makes

vehicles keep a safe distance with each other, which can help vehicle travel through the intersection without stop. In the benchmark algorithm, since the vehicle enters the cooperative zone, it tries to decelerate continuously for getting reservation, casing a mismatched time window and resulting in the vehicle not being reserved. The average waiting time is increasing drastically when the traffic density is greater than 70 m/veh.

Therefore, compared with the benchmark algorithm, the distributed control method can not only reduce vehicle fuel consumption and improve traffic efficiency under different traffic flow densities, but also increase the critical density of congestion, which significantly alleviates traffic congestion. From the results, although we cannot explicitly see the impact of the communication structure, we can see that the communication among a limited number of vehicles can ensure the platoon stability and follow-up safety.

VII. CONCLUSION

This paper constructed a distributed cooperative control method for non-signalized intersection networks. We extended the geometric configuration of the original single-point virtual platoon to the case of road networks. Then the geometric configuration for vehicle groups in the road network was constructed, which included geometric topologies for vehicle platoons in road segments and vehicle groups at intersections. In order to ensure that vehicles converged to a steady state quickly, based on the vehicle following behavior characteristics in the vehicle groups, we proposed a method of geometric topology splitting and combination of the vehicle groups. The maneuver for each CAVs was designed by the cooperative framework under communication. In other words, CAVs traveled at the desired speed computed by a distributed controller. The distributed controller considers the collision-free geometric topology of the virtual platoon, communication topology, vehicle dynamics, and distributed feedback law, constructing aggregate dynamics model of virtual vehicle platoons, which helped vehicles to avoid collisions with each other and improve vehicles speed. We also provided an example implementation of the scheme and compared its performance with the FCFS benchmark algorithm through microscopic traffic simulations under various demand levels. Test results showed that the distributed cooperative control method can significantly improve vehicle fuel economy and traffic efficiency at different traffic flow densities. In addition, since the speeds of vehicles near the intersection were adjusted, the number of stops was reduced to zero.

As the next important step, it will be interesting in the future to expand the methodology to include different CAVs penetration rates. Therefore, mixed traffic of autonomous and human-driven vehicles is worth studying. As a suggestion, the platoon modeling can be reconstructed that the formation of human-driven vehicles is with a leader of an autonomous vehicle.

REFERENCES

[1] J. Lioris, R. Pedarsani, F. Y. Tascikaraoglu, and P. Varaiya, "Platoons of connected vehicles can double throughput in urban roads," *Transp. Res. C, Emerg. Technol.*, vol. 77, pp. 292–305, Apr. 2017, doi: 10.1016/j.trc.2017.01.023.

[2] D. Xie, X. Zhao, and Z. He, "Heterogeneous traffic mixing regular and connected vehicles: Modeling and stabilization," *IEEE Trans. Intell. Transp. Syst.*, vol. 20, no. 6, pp. 2060–2071, Aug. 2018, doi: 10.1109/TITS.2018.2857465.

[3] J. Ploeg, D. P. Shukla, N. van de Wouw, and H. Nijmeijer, "Controller synthesis for string stability of vehicle platoons," *IEEE Trans. Intell. Transp. Syst.*, vol. 15, no. 2, pp. 854–865, Apr. 2014, doi: 10.1109/TITS.2013.2291493.

[4] B. Xu, X. J. Ban, Y. Bian, W. Li, and J. Wang, "Cooperative method of traffic signal optimization and speed control of connected vehicles at isolated intersections," *IEEE Trans. Intell. Transp. Syst.*, vol. 20, no. 4, pp. 1390–1403, Jul. 2018, doi: 10.1109/TITS.2018.2849029.

[5] S. Bae, Y. Kim, J. Guanetti, F. Borrelli, and S. Moura, "Design and implementation of ecological adaptive cruise control for autonomous driving with communication to traffic lights," 2018, *arXiv:1810.12442*. [Online]. Available: http://arxiv.org/abs/1810.12442

[6] J. Zheng and H. X. Liu, "Estimating traffic volumes for signalized intersections using connected vehicle data," *Transp. Res. C, Emerg. Technol.*, vol. 79, pp. 347–362, Jun. 2017, doi: 10.1016/j.trc.2017.03.007.

[7] O. Younis and N. Moayeri, "Employing cyber-physical systems: Dynamic traffic light control at road intersections," *IEEE Internet Things J.*, vol. 4, no. 6, pp. 2286–2296, Dec. 2017, doi: 10.1109/JIOT.2017.2765243.

[8] B. Xu, F. Zhang, J. Wang, and K. Li, "B&B algorithm-based green light optimal speed advisory applied to contiguous intersections," in *Proc. CICTP*, Jul. 2015, pp. 363–375, doi: 10.1061/9780784479292.033.

[9] S. Xu and H. Peng, "Design and comparison of fuel-saving speed planning algorithms for automated vehicles," *IEEE Access*, vol. 6, pp. 9070–9080, 2018, doi: 10.1109/ACCESS.2018.2805883.

[10] Q. Lin, S. E. Li, X. Du, X. Zhang, H. Peng, Y. Luo, and K. Li, "Minimize the fuel consumption of connected vehicles between two red-signalized intersections in urban traffic," *IEEE Trans. Veh. Technol.*, vol. 67, no. 10, pp. 9060–9072, Oct. 2018, doi: 10.1109/TVT.2018.2864616.

[11] Y. Fu, C. Li, T. H. Luan, Y. Zhang, and G. Mao, "Infrastructure-cooperative algorithm for effective intersection collision avoidance," *Transp. Res. C, Emerg. Technol.*, vol. 89, pp. 188–204, Apr. 2018, doi: 10.1016/j.trc.2018.02.003.

[12] A. Talebpour and H. S. Mahmassani, "Influence of connected and autonomous vehicles on traffic flow stability and throughput," *Transp. Res. C, Emerg. Technol.*, vol. 71, pp. 143–163, Oct. 2016, doi: 10.1016/j.trc.2016.07.007.

[13] Y. Feng, C. Yu, and H. X. Liu, "Spatiotemporal intersection control in a connected and automated vehicle environment," *Transp. Res. C, Emerg. Technol.*, vol. 89, pp. 364–383, Apr. 2018, doi: 10.1016/j.trc.2018.02.001.

[14] N. Lu, N. Cheng, N. Zhang, X. Shen, and J. W. Mark, "Connected vehicles: Solutions and challenges," *IEEE Internet Things J.*, vol. 1, no. 4, pp. 289–299, Aug. 2014, doi: 10.1109/JIOT.2014.2327587.

[15] F. Zhu, H. M. A. Aziz, X. Qian, and S. V. Ukkusuri, "A junction-tree based learning algorithm to optimize network wide traffic control: A coordinated multi-agent framework," *Transp. Res. C, Emerg. Technol.*, vol. 58, pp. 487–501, Sep. 2015, doi: 10.1016/j.trc.2014.12.009.

[16] N. J. Goodall, B. L. Smith, and B. Park, "Traffic signal control with connected vehicles," *Transp. Res. Rec., J. Transp. Res. Board*, vol. 2381, no. 1, pp. 65–72, Jan. 2013, doi: 10.3141/2381-08.

[17] B. Asadi and A. Vahidi, "Predictive cruise control: Utilizing upcoming traffic signal information for improving fuel economy and reducing trip time," *IEEE Trans. Control Syst. Technol.*, vol. 19, no. 3, pp. 707–714, May 2011, doi: 10.1109/TCST.2010.2047860.

[18] H. Jiang, J. Hu, S. An, M. Wang, and B. B. Park, "Eco approaching at an isolated signalized intersection under partially connected and automated vehicles environment," *Transp. Res. C, Emerg. Technol.*, vol. 79, pp. 290–307, Jun. 2017, doi: 10.1016/j.trc.2017.04.001.

[19] X. He, H. X. Liu, and X. Liu, "Optimal vehicle speed trajectory on a signalized arterial with consideration of queue," *Transp. Res. C, Emerg. Technol.*, vol. 61, pp. 106–120, Dec. 2015, doi: 10.1016/j.trc.2015.11.001.

[20] K. Dresner and P. Stone, "Multiagent traffic management: An improved intersection control mechanism," in *Proc. 4th Int. Joint Conf. Auto. Agents Multiagent Syst.*, 2005, pp. 530–537.

[21] K. Dresner and P. Stone, "A multiagent approach to autonomous intersection management," *J. Artif. Intell. Res.*, vol. 31, pp. 591–656, Mar. 2008.

[22] K. Zhang, D. Zhang, A. de La Fortelle, X. Wu, and J. Gregoire, "State-driven priority scheduling mechanisms for driverless vehicles approaching intersections," *IEEE Trans. Intell. Transp. Syst.*, vol. 16, no. 5, pp. 2487–2500, Oct. 2015, doi: 10.1109/TITS.2015.2411619.
[23] J. Lee and B. Park, "Development and evaluation of a cooperative vehicle intersection control algorithm under the connected vehicles environment," *IEEE Trans. Intell. Transp. Syst.*, vol. 13, no. 1, pp. 81–90, Mar. 2012, doi: 10.1109/TITS.2011.2178836.
[24] B. Xu, S. E. Li, Y. Bian, S. Li, X. J. Ban, J. Wang, and K. Li, "Distributed conflict-free cooperation for multiple connected vehicles at unsignalized intersections," *Transp. Res. C, Emerg. Technol.*, vol. 93, pp. 322–334, Aug. 2018, doi: 10.1016/j.trc.2018.06.004.
[25] D. Kim and O. Jeong, "Cooperative traffic signal control with traffic flow prediction in multi-intersection," *Sensors*, vol. 20, no. 1, p. 137, Dec. 2019, doi: 10.3390/s20010137.
[26] H. Ge, Y. Song, C. Wu, J. Ren, and G. Tan, "Cooperative deep Q-learning with Q-value transfer for multi-intersection signal control," *IEEE Access*, vol. 7, pp. 40797–40809, 2019, doi: 10.1109/ACCESS.2019.2907618.
[27] Y. J. Zhang, A. A. Malikopoulos, and C. G. Cassandras, "Optimal control and coordination of connected and automated vehicles at urban traffic intersections," in *Proc. Amer. Control Conf. (ACC)*, Jul. 2016, pp. 6227–6232, doi: 10.1109/ACC.2016.7526648.
[28] J. Z. Zhu, J. X. Cao, and Y. Zhu, "Traffic volume forecasting based on radial basis function neural network with the consideration of traffic flows at the adjacent intersections," *Transp. Res. C, Emerg. Technol.*, vol. 47, pp. 139–154, Oct. 2014, doi: 10.1016/j.trc.2014.06.011.
[29] F. Ashtiani, S. A. Fayazi, and A. Vahidi, "Multi-intersection traffic management for autonomous vehicles via distributed mixed integer linear programming," in *Proc. Annu. Amer. Control Conf. (ACC)*, Jun. 2018, pp. 6341–6346, doi: 10.23919/ACC.2018.8431656.
[30] Y. Wang, P. Cai, and G. Lu, "Cooperative autonomous traffic organization method for connected automated vehicles in multi-intersection road networks," *Transp. Res. C, Emerg. Technol.*, vol. 111, pp. 458–476, Feb. 2020, doi: 10.1016/j.trc.2019.12.018.
[31] S. E. Li, Y. Zheng, K. Li, L.-Y. Wang, and H. Zhang, "Platoon control of connected vehicles from a networked control perspective: Literature review, component modeling, and controller synthesis," *IEEE Trans. Veh. Technol.*, early access, Jul. 6, 2017, doi: 10.1109/TVT.2017.2723881.
[32] Y. Jiang, S. Li, and D. E. Shamo, "A platoon-based traffic signal timing algorithm for major–minor intersection types," *Transp. Res. B, Methodol.*, vol. 40, no. 7, pp. 543–562, Aug. 2006, doi: 10.1016/j.trb.2005.07.003.
[33] H. Hao and P. Barooah, "Stability and robustness of large platoons of vehicles with double-integrator models and nearest neighbor interaction," *Int. J. Robust Nonlinear Control*, vol. 23, no. 18, pp. 2097–2122, Dec. 2013, doi: 10.1002/rnc.2872.
[34] P. N. Shivakumar and K. H. Chew, "A sufficient condition for nonvanishing of determinants," *Proc. Amer. Math. Soc.*, vol. 43, no. 1, pp. 63–66, 1974, doi: 10.2307/2039326.
[35] R. A. Horn and C. R. Johnson, *Matrix Analysis*, 2nd ed. New York, NY, USA: Cambridge Univ. Press, 2012.
[36] D. Krajzewicz, J. Erdmann, M. Behrisch, and L. Bieker, "Recent development and applications of SUMO-Simulation of Urban MObility," *Int. J. Adv. Syst. Meas.*, vol. 5, no. 3, p. 4, 2012.
[37] Z. Li, M. V. Chitturi, D. Zheng, A. R. Bill, and D. A. Noyce, "Modeling reservation-based autonomous intersection control in VISSIM," *Transp. Res. Rec., J. Transp. Res. Board*, vol. 2381, no. 1, pp. 81–90, Jan. 2013.

XIAOLONG CHEN received the B.E. degree from the College of Mechanical and Automation, Fuzhou University, in 2016, and the master's degree from the College of Mechanical and Vehicle Engineering, Hunan University, where he is currently pursuing the Ph.D. degree. His research interests include distributed cooperative control method of connected and automated vehicles and multi-agent control.

BIAO XU (Member, IEEE) received the B.E. and Ph.D. degrees from Tsinghua University, Beijing, China, in 2013 and 2018, respectively.

From 2016 to 2017, he was a Visiting Scholar with the University of Washington, Seattle, WA, USA. He is currently an Associate Research Fellow at the College of Mechanical and Vehicle Engineering, Hunan University. His active research interests include connected and automated vehicles, vehicle control, and V2I cooperation. He was a recipient of the Best Paper Award in 14th Intelligent Transportation Systems Asia-Pacific Forum in 2015, and the Best Paper Award in the 2017 IEEE Intelligent Vehicle Symposium.

XIAOHUI QIN received the B.E. and Ph.D. degrees from Tsinghua University, Beijing, China, in 2010 and 2016, respectively.

From 2011 to 2012, he was a Visiting Scholar with the Polytechnic University of Milan, Milan, Italy. He is currently an Associate Research Fellow at the College of Mechanical and Vehicle Engineering, Hunan University. His research interests include cooperative platoon control and SLAM.

YOUGANG BIAN (Member, IEEE) received the B.E. and Ph.D. degrees from Tsinghua University, in 2014 and 2019, respectively. From 2017 to 2018, he was a Visiting Student with the Department of Electrical and Computer Engineering, University of California at Riverside. His research interests include distributed control of dynamical systems with its applications to connected and automated vehicles. He received the Best Paper Award at the 2017 IEEE Intelligent Vehicles Symposium.

MANJIANG HU received the B.Tech. and Ph.D. degrees from Jiangsu University, China, in 2009 and 2014, respectively.

He held a postdoctoral position at the Department of Automotive Engineering, Tsinghua University, from 2014 to 2017. He is currently a Research Fellow with the College of Mechanical and Vehicle Engineering, Hunan University. His research interests include cooperative driving assistance technology and vehicle control.

NING SUN received the Ph.D. degree from Jiangsu University, Zhenjiang, China, in 2018.

She currently holds a postdoctoral position at the School of Mechanical and Vehicle Engineering, Hunan University, Changsha. She was specialized in vehicle active safety technology and intelligent vehicles.